

Study of 20-inch PMTs dark count generated large pulses

Yu Zhang,^{a,b,c} Zhimn Wang,^{a,b,c,1} Min Li,^{a,b,c} Yongpeng Zhang,^{a,b,c} Yaoguang Wang,^a
Zhaoyuan Peng,^{a,b,c} Changgen Yang,^{a,b} Yuekun Heng^{a,b,c}

^a*Institute of High Energy Physics, Beijing 100049, China*

^b*University of Chinese Academy of Sciences, Beijing 100049, China*

^c*State Key Laboratory of Particle Detection and Electronics, Beijing 100049, China*

E-mail: wangzhm@ihep.ac.cn

ABSTRACT: The main goal of the JUNO experiment is to determine the neutrino mass ordering with a 20 kt liquid-scintillator detector. The 20-inch PMT is crucial as one of JUNO key instruments to realize an excellent energy resolution of at least 3% at 1 MeV. The knowledge on PMT's characterisation and feature is critical for detector performance understanding. Large pulses from PMT dark count such as from flasher or others are one of the serious concerns for detector noise control. Focusing on the large pulses from 20-inch PMT dark count, this paper is trying to investigate the causes by measurements with a muon tagging system. It is found that the large pulses of 20-inch PMT dark count is contributed mainly from muons hitting the PMT glass. A simulation is also realized and achieved a consistent understanding.

KEYWORDS: photon detectors for UV, visible and IR photons (vacuum) (photomultipliers, HPDs, others), PMT, MCP-PMT, cosmic ray, glass Cerenkov light

ARXIV EPRINT: [1234.56789](https://arxiv.org/abs/1234.56789)

¹Corresponding author.

Contents

1	Introduction	1
2	Experimental setup	2
2.1	Testing System	2
2.2	PMT settings	4
3	Measurement results	6
3.1	Dark count	7
3.1.1	Dark count rate (DCR)	7
3.1.2	Dark count waveform	8
3.2	Muon hit PMT glass	8
3.2.1	20-inch PMT coincidence only with PS1	10
3.2.2	PMT photocathode down	12
4	Simulation	12
4.1	Simulation setup	12
4.1.1	Effect of glass thickness and QE	14
4.1.2	Simulation for muons	15
4.2	Comparison of PMT photocathode up and down	16
5	Summary	17

1 Introduction

The Jiangmen Underground Neutrino Observatory (JUNO) [1, 2] is under construction at Jiangmen, Guangdong, China. The experiment aims to study neutrino mass ordering with 3% energy resolution at 1 MeV, a precise determination of neutrino oscillation parameters, and other neutrino physics with 20kton liquid scintillator viewed by up to 20,000 high quantum efficiency (QE) 20-inch PMTs. JUNO selected two kinds of 20-inch PMTs whose typical photon detection efficiency higher than 27% [3–5]: 5,000 of Hamamatsu Photonics K.K. (HPK, R12860) dynode PMT [6] and 15,000 of the newly developed MCP PMT from North Night Vision Technology Co., LTD (NNVT, GDB6201) [7], as shown in Fig. 1.

Photomultiplier tubes (PMT) are widely used in particle physics experiments for the light detection sensitive to single photon, such as Super-K [8, 9], KamLAND [10], SNO [11], MiniBoone [12], Icecube [13], Chooz [14], Daya Bay [15], and RENO [16]. PMT’s performance and its characters have been studied in detail with well understanding [5, 17–29]. Some large pulses of PMT made a lot of trouble to recent world-wide rare event neutrino experiments, and additional analysis strategy is introduced to suppress its effect, such as

Double Chooz[30], Daya Bay[31], Icecube[32] and RENO[33]. Additional studies are done on flasher and large pulses already as in [34, 35]. It is also valuable to mention that the flashers from PMT HV divider of JUNO is studied in [25]. As known, it will generate a large pulse by Cerenkov radiation when a muon is crossing through the PMT glass (Hamamatsu PMT R5912) as studied in [36, 37]. PMT large pulse still needs further study to identify either flasher or others to have a better rejection to noise, in particular for the 20-inch PMTs and the coming rare event detection projects, such as JUNO[1, 2], HyperK[38, 39].



Figure 1: Photograph of JUNO selected 20-inch NNVT MCP PMT (left) and HPK dynode PMT (right).

In this article, we will show a detailed study on the large pulses of 20-inch PMT associated with muon tagged by a plastic scintillator coincidence system. Sec. 2 will provide a short description on the testing system and configurations. Sec. 3 will show the measurement results under different conditions. A dedicated simulation is done for better understanding and comparing with the measurements as shown in Sec. 4. Finally, a short summary is reached in Sec. 5.

2 Experimental setup

For better pressure tolerance of both types of JUNO selected PMTs, the thickness is designed larger for most part of the glass bulb. The typical glass thickness¹ is measured with few PMT samples as shown in Fig. 2, which is thicker than the widely used Hamamatsu R5912 1-3 mm [41]. Considering the huge dimension, high QE and larger thickness of the glass bulb of the JUNO selected 20-inch PMTs, it is expected to have a higher muon hitting rate at sea level and stronger Cerenkov light intensity for a muon passing through the glass.

2.1 Testing System

A muon coincidence system is used to identify the 20" PMT's pulse correlated with muons from different directions by two plastic scintillators as shown in Fig. 3. A muon will be

¹The thickness of 20-inch NNVT PMT and HPK PMT glass at different positions is measured by an ultrasonic thickness gauge TT112[40].

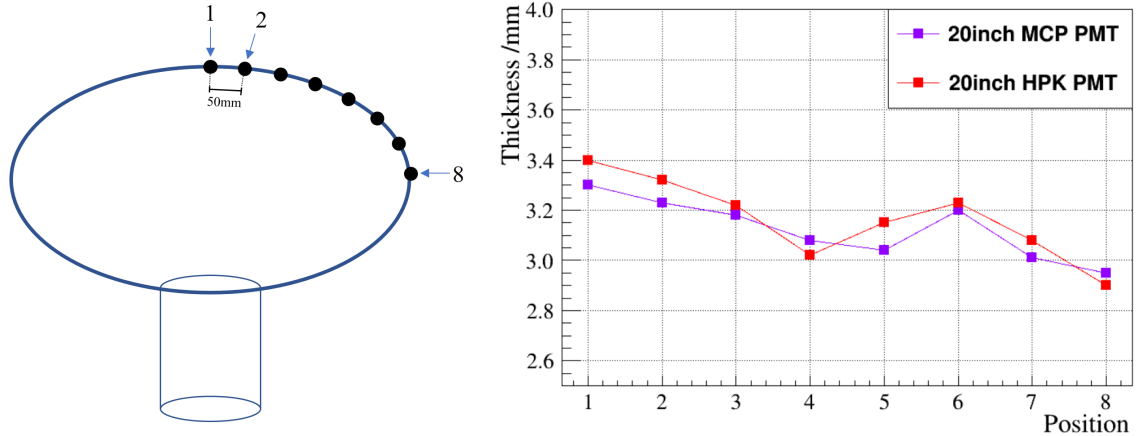


Figure 2: Glass thickness of the photocathode hemisphere of 20-inch PMTs. Left: measurement positions at different zenith angles; right: the measured glass thickness of HPK and NNVT PMTs.

tagged by the coincidence of the two plastic scintillators (PS1 and PS2, distance in height is around 80 cm) to select the muons going through the glass bulb of the 20-inch PMT. The dimension of the scintillators is $22 \times 32.5 \times 5 \text{ cm}^3$ for PS1, and $16 \times 35 \times 1 \text{ cm}^3$ for PS2, respectively. PMT XP2020 [42], coupled to the scintillators by light guide, has a very narrow width of its output pulse (FWHM $\sim 2.4 \text{ ns}$), which is much smaller than the 20-inch PMTs (FWHM $7 \sim 10 \text{ ns}$). The PS1 will be moved to several locations to select muons with different incident angles, and the 20-inch PMT can be placed with glass bulb up (as shown in Fig. 3) or glass bulb down to check the effect of the Cerenkov light direction. The waveforms of the three signal channels from the two scintillators and the 20-inch PMT will be acquired in a same time window following the coincidence trigger by a digitizer of CAEN DT5751 [43], which has 1 GSample/s, 1 Vpp dynamic range with 1 mV precision under 50Ω impedance. The power of all the used PMTs is supplied by a SHR desktop HV module [44]. More detailed information on the signals' processing electronics is shown in Fig. 4, where few electronics modules are used for signal splitting (Linear FIFO CAEN Mod. N625 [45]), $\times 10$ fast amplification (CAEN Mod. N979 [46]), low threshold discrimination (CAEN Mod. N845 [47]), logic counter (CAEN Mod. N1145 [48]), and logic coincidence (CAEN Mod. N455 [49]).

The coincidence window length used for trigger generation is set to 100 ns, and the window length of the waveform data taking is selected to $1 \mu\text{s}$, where the primary signal is shifted to around 450-650 ns for both scintillators and 20-inch PMT. Furthermore, the system can be set to several trigger configurations manually (trigger mode):

1. Triggered by only one of the three signal channels (PMTs) for the measurement of dark count, mainly for the 20-inch PMT.
2. Triggered by two-coincidence of PS1 and 20-inch PMT for muon and gammas which passes the 20-inch PMT.

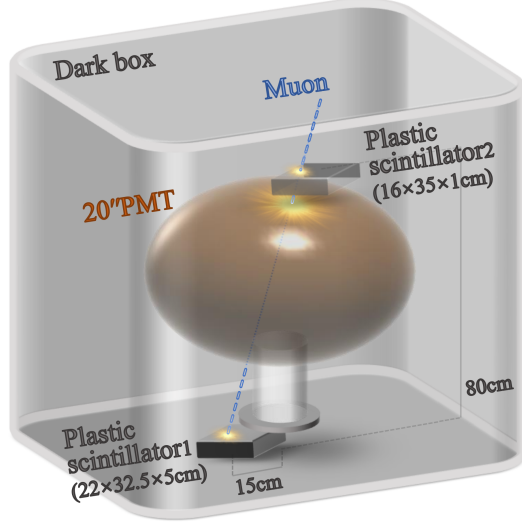


Figure 3: Layout of the 20-inch PMT's large pulse testing system with muon tracking scintillators.

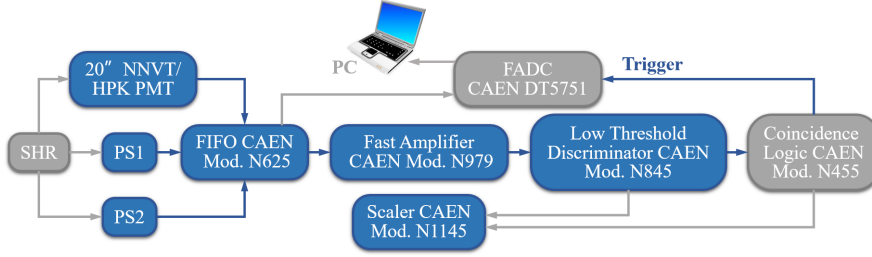


Figure 4: Electronics system used for the large pulse testing of 20-inch PMT dark count.

3. Triggered by triple-coincidence of PS1, PS2 and 20-inch PMT for purer muon which passes 20-inch PMT.

With the record waveforms, a charge integration window of 20-inch PMT is selected relative to the peak location of the primary pulse in $[-15,45]$ ns for NNVT PMT and $[-15,50]$ ns for HPK PMT, while the window for baseline is shifted before the primary pulse by 100 ns and selected in $[-115,-55]$ ns and $[-115,-50]$ ns respectively as shown in Fig. 5. The hit time, pulse amplitude will be derived from the waveform too. The signal of plastic scintillators is processed similar to the 20-inch PMT.

2.2 PMT settings

The 20-inch PMT is working with an optimized HV divider and positive HV [50, 51]. The working point of the 20-inch PMT is aiming to be around a gain of 1×10^7 for both types of PMTs to simulate the future JUNO conditions. Following the traditional PMT gain calibration methods, such as a DC current-based method [52], charge spectrum method with pulse light source [53, 54], and gain determination algorithms [55, 56], a method (peak

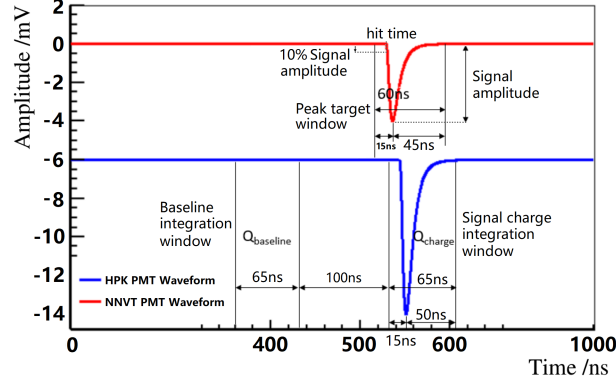


Figure 5: Exemplary of signal waveforms (simulation, with artificial offset): the charge integration window for baseline and signal, hit time, and pulse amplitude. Red: NNVT PMT; blue, HPK PMT.

gain) based on the peak of single photoelectron (SPE) spectrum from dark count events is used to simplify the testing and analysis process.

Derived from the measured SPE spectra of charge and amplitude of 20-inch PMTs as shown in Fig. 6, the SPE amplitude is around 7.0 mV for NNVT PMT with a gain of 1.2×10^7 and 6.0 mV for HPK PMT with a gain of 1.0×10^7 . An analysis threshold in amplitude of 3 mV is used for both types of PMTs, and the calibrated gain is used for the photoelectron calculation. The dark count rate (DCR) is also measured under the setting point with a quarter p.e. threshold² here. It is around 16 kHz for NNVT PMT and 44 kHz for HPK PMT respectively, where a tiny light leakage in single photon level (around 20-30 kHz) is found during the testing of HPK PMT from the used black cloth covering of the system.

A similar procedure is applied to the PMTs of the scintillators, a working point is settle down too. The amplitude of SPE is around 4.3 mV for PS1 and 5.4 mV for PS2, and the gain is 0.35×10^7 for PS1 and 0.34×10^7 for PS2 respectively. The relationship between the amplitude and charge gain is different to the 20-inch PMTs, which is mainly from the shape features of the pulses as discussed in Sec. 2.1. The count rate of the scintillators with PMT is also measured with an amplitude threshold around 30 mV (without amplifier), it is around 3 kHz for PS1 and 1 kHz for PS2 respectively. The measured charge spectra of the plastic scintillators are shown in Fig. 7, where the typical effective light yield to muon is around 140 p.e. for PS1 and 40 p.e. for PS2. The differences on counting rate and muon response all come from the thickness of the scintillators. Another offline charge cut of scintillaotrs will be used for more purer muon selection: 70 p.e. for PS1 and 20 p.e. for PS2³. All the measured parameters are shown in Tab. 1.

²The threshold is also used for the following muon related testing.

³The threshold is settle done on balance to remove the gammas and to keep a higher muon detection efficiency.

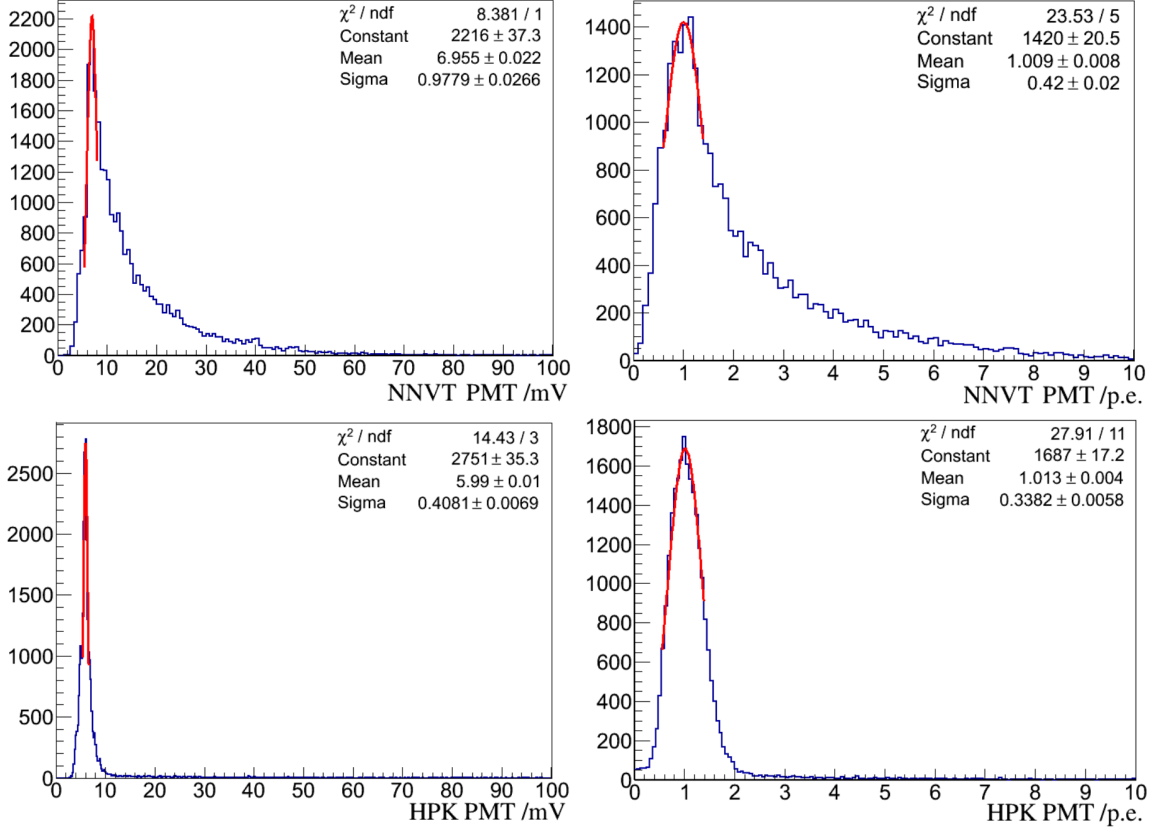


Figure 6: Measured SPE spectra of 20-inch HPK or NNVT PMTs, where a Gaussian fit in red line is applied around the peaks. Top left: MCP PMT SPE amplitude spectrum; top right: MCP PMT SPE charge spectrum; bottom left: HPK PMT SPE amplitude spectrum; bottom right: HPK PMT SPE charge spectrum. Note that the calibrated PMT gain is used for the charge calculation in p.e..

Table 1: Setting point of all the PMTs

PMT	HV (V)	SPE amplitude (mV)	Gain ($\times 10^7$)	Count rate (kHz)
20-inch NNVT	1770	7.0	1.20	16
20-inch HPK	1677	6.0	1.00	44
PMT1 w/ PS1	-2200	4.3	0.35	3
PMT2 w/ PS2	-1800	5.4	0.34	1

3 Measurement results

Except the rate of dark count of 20-inch PMT, more features are measured for better understanding on it, such the dark count rate (DCR) versus threshold, the amplitude and charge spectra to understand the sources of dark count, such as sources from thermal

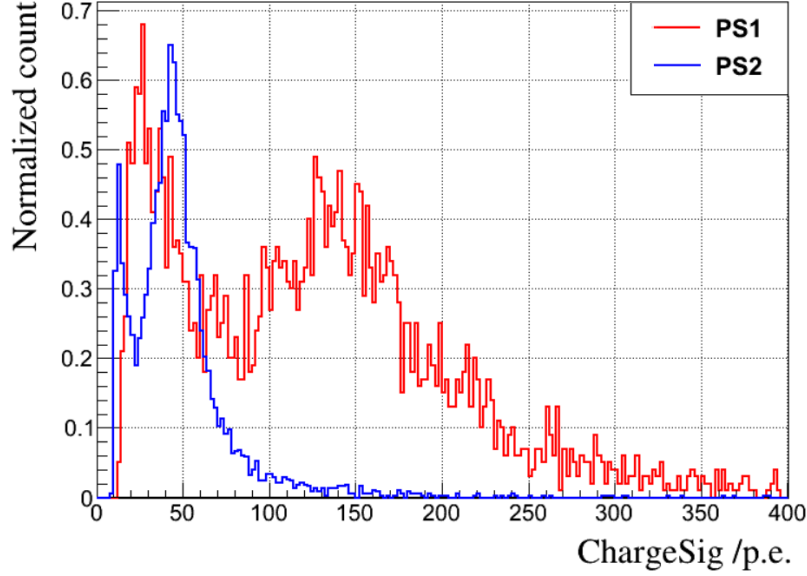


Figure 7: Measured charge spectra of scintillators which are measured with a threshold around 10 p.e. The response difference comes from their thickness as stated.

emission, muons, natural radioactivity, or flashers.

In this section, a detailed measurement on the dark count of 20-inch PMT is done firstly. Then, the dark count related to muons is further measured under several configurations. All the results will be discussed one by one.

3.1 Dark count

3.1.1 Dark count rate (DCR)

Dark count is mainly source from the thermal electron emission of PMT photocathode in dark. Its amplitude should be in SPE level normally [52, 57], which is mostly less than 3 p.e. and $\ll 1$ Hz for > 3 p.e. (assuming DCR in SPE ~ 10 kHz and 10 ns coincidence window). A threshold survey is done for the dark count rate of 20-inch PMT as shown in Fig. 8. Due to the tightness of the device, there is a tiny light leakage during HPK PMT measurement as mentioned, which results in a higher count rate when the threshold less than 10 mV. Comparing with expectation, it is clear that there shows an obvious rate when the threshold is higher than 20 mV (around 3 p.e. according to Tab. 1), even higher than 50 mV (around 10 p.e.) in amplitude for both types of PMTs. It is over the contribution only from the thermal noise about the DCR. The higher rate of large pulses of NNVT PMT than HPK PMT is related to the response features of NNVT PMT on amplitude as shown in Fig. 6, where the NNVT PMT shows a wider distribution on amplitude than HPK PMT even both of them in SPE level.

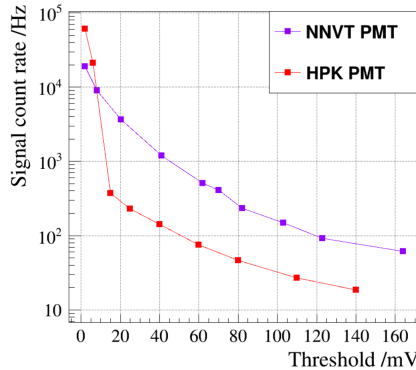


Figure 8: Dark count rate of 20-inch PMTs vs. threshold.

3.1.2 Dark count waveform

The waveforms are further taken during the threshold survey for both types of PMTs with the system⁴. The distributions of DCR amplitude and charge are shown in Fig. 9, where all the plots are normalized to the lowest threshold result according to the event numbers higher than 200 mV. All the spectra of amplitude (charge) of both types of PMTs are following a similar overall trend, and showing a structure in steps, in amplitude (charge):

1. The first step from 0 to ~ 10 mV (0 to ~ 3 p.e. in charge), which should be mainly contributed by the thermal electron emission. The result of HPK PMT suffers from the tiny light leakage.
2. The second step from ~ 10 mV to ~ 100 mV (~ 3 p.e. to ~ 20 p.e. in charge), which still needs further understanding.
3. The third step from ~ 100 mV to ~ 500 mV (~ 20 p.e. to at least ~ 150 p.e. in charge), which still needs further understanding, which this study is trying to focus on.

3.2 Muon hit PMT glass

With the system, trigger mode #3 (triple coincidence of PSs and 20-inch PMT, see Sec. 2.1) is used for muon related signal testing. The parameters (see Fig. 5) are derived from the measured waveforms. The hit-time correlation of both PSs (shown on the left of Fig. 10) is checked firstly to exclude possible random noise, where only the events around [470,510] ns of x-axis and [500,530] ns of y-axis are selected for the following analysis. The hit-time correlation between PS1 and 20-inch PMT (shown on the right of Fig. 10) is also selected in the similar way for the following analysis.

When the PS1 located at the position 0.15 m relative to the central axis of 20-inch PMT (zenith angle (θ) of muon incident is around $27^\circ \pm 16^\circ$), the measured charge spectra after hit-time cut (tagged by "Trigger #3") of 20-inch MCP PMT can be found on the left of Fig. 11, where the charge spectrum of dark count (trigger mode #1, tagged by "PMT

⁴The data taking dead time is assumed to be random even for high enough trigger rate, and no systematic effect on the overall distribution.

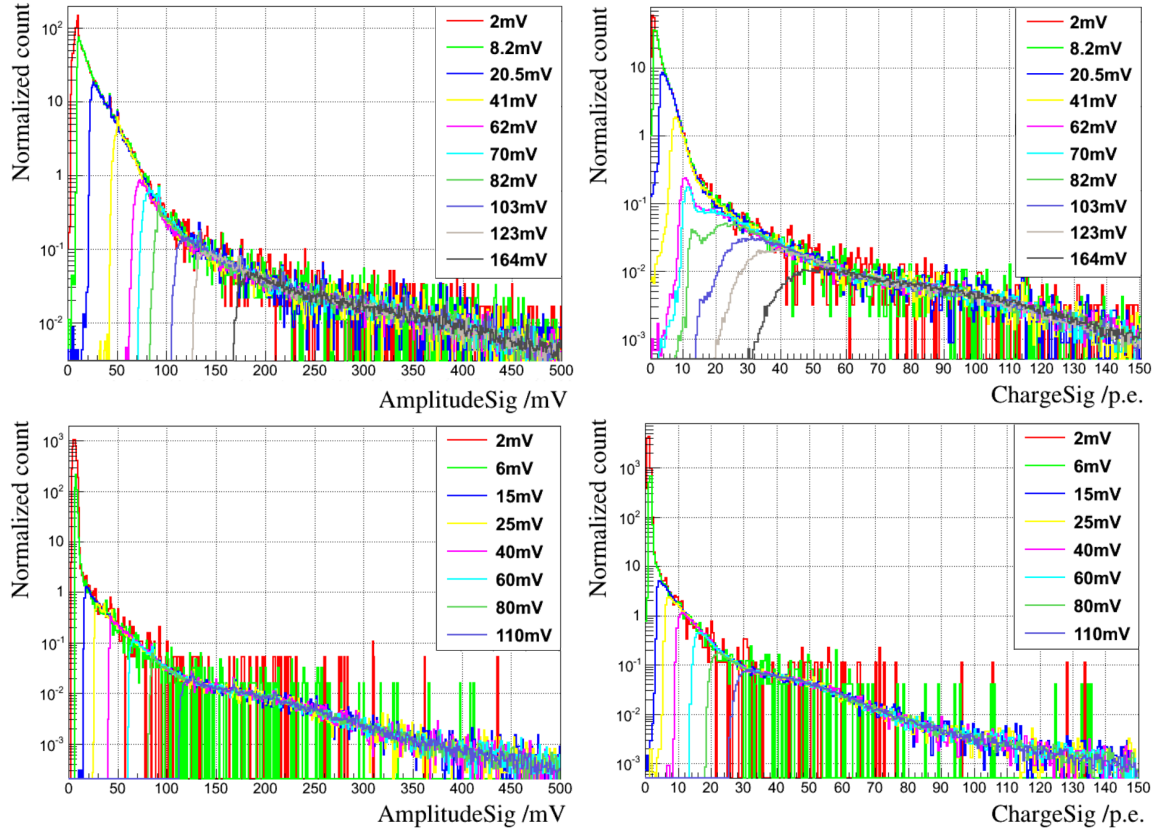


Figure 9: The normalized amplitude (left) and charge (right) spectra of 20-inch PMTs' dark count at different thresholds. Top left: 20-inch NNVT PMT amplitude spectrum; top right: 20-inch NNVT PMT charge spectrum; bottom left: 20-inch HPK PMT amplitude spectrum; bottom right: 20-inch HPK PMT charge spectrum.

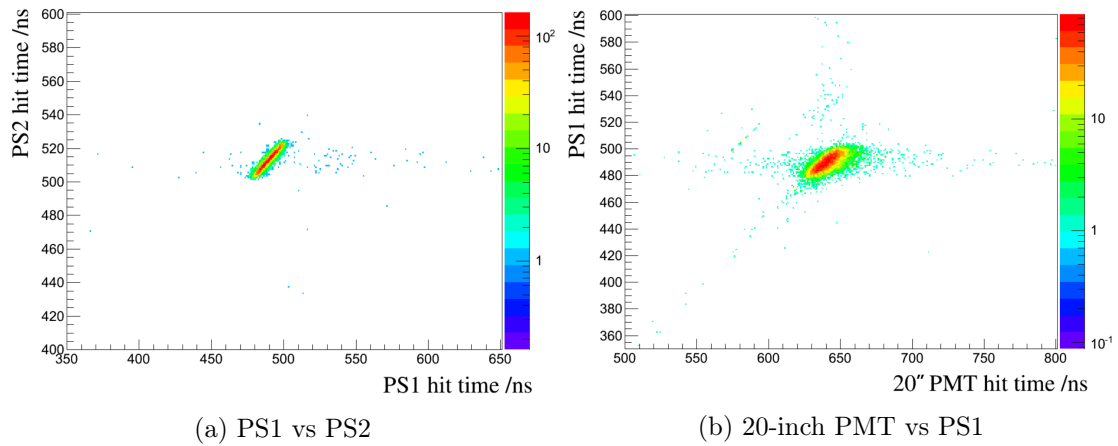


Figure 10: 2D hit-time correlation between the two scintillators (left) and PS1 and 20-inch PMT (right).

dark count") is also shown on the same figure. A further selected spectrum after the offline charge cut of PSs (tagged by "Trigger #3 w/ PS cut") is drawn on the same figure. All the curves are normalized according to the large pulse events of dark count spectrum. Firstly, it is found on the left of Fig. 11 for NNVT PMT that the muon related events are mainly related to the large pulses with typical charge around 76 p.e. – the step 3 as discussed in Sec. 3.1.2. Secondly, the muon related events also contribute to part of lower than 40 p.e. located at the step 2 as discussed in Sec. 3.1.2. Similar features can be identified for the 20-inch HPK PMT as shown on the right of Fig. 11, where the typical signal intensity in charge is around 30 p.e. located at the step 3 too. It is clear that the muon related events mainly contribute to the entries of step 3, and partially contribute to the step 2.

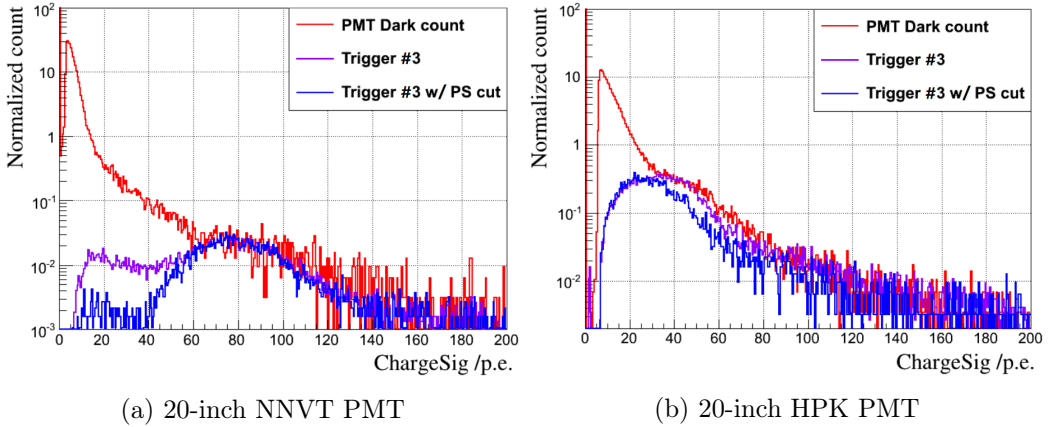


Figure 11: Measured charge spectra of 20-inch PMTs. Left: MCP PMT; right: HPK PMT. Red: Dark count spectrum (tagged by "PMT dark count"), same as in Fig. 9; purple: the measured spectrum selected only with the hit time cut of PSs; blue: after offline charge cut.

In order to survey more directions of muons going through the 20-inch PMT, another two data sets are taken when PS1 located at 0.5 m (zenith angle (θ) is around $43^\circ \pm 11^\circ$) and 1.0 m (zenith angle (θ) is around $58^\circ \pm 7^\circ$) relative to the 20-inch PMT central axis. The measured charge spectra after PSs' offline charge cut are shown in Fig. 12 for both types of PMTs. All the measurements provide consistent results on the muon related signal strength, while the difference mainly focus on the measured event rate from solid angle. The measured muon rate by PMT only is selected with charge larger than 50 p.e. for NNVT PMT and larger than 10 p.e. for HPK PMT, respectively. The typical charge strength and event rate are collected and summarized in Tab. 2, where the rate is related to the specified arrangement layout of the location of the two scintillators during each measurement, which could have some uncertainty, especially for PS1.

3.2.1 20-inch PMT coincidence only with PS1

Another configuration with trigger mode #2 (20-inch PMT coincidence only with PS1, see Sec. 2.2) is used for the measurements with 20-inch PMT for cross check of muon related events, where PS1 is located at 0.15 m relative to the PMT central axis. The 2-D hit-time

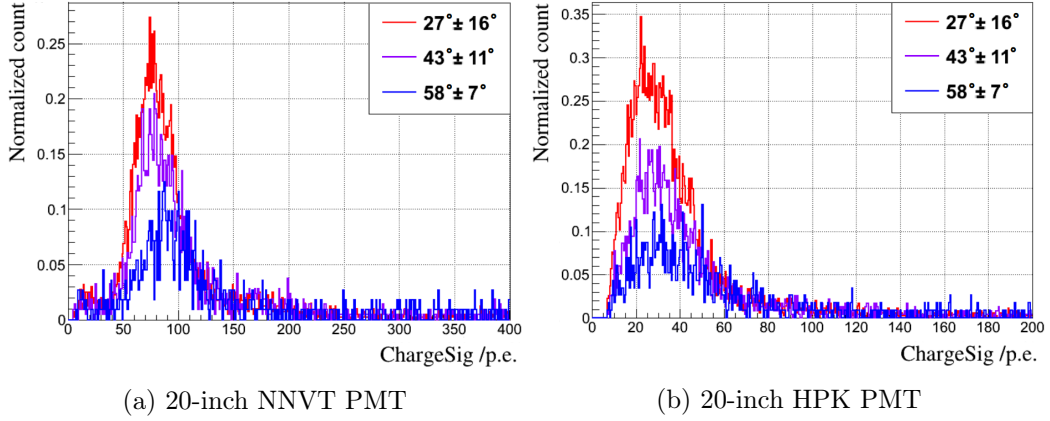


Figure 12: Measured charge spectra of 20-inch PMTs in different muon directions. Left: 20-inch NNVT PMT; right: 20-inch HPK PMT. Red: zenith angle (θ) is around $27^\circ \pm 16^\circ$; purple: zenith angle (θ) is around $43^\circ \pm 11^\circ$; blue: zenith angle (θ) is around $58^\circ \pm 7^\circ$.

Table 2: Event strength and rate of different muon directions

Configuration	PMT	rate w/ one PS (w/ PS cut) (Hz) (w/ PS ,w/ PMT cut)	rate w/ double PSs (w/ PS cut) (Hz) (w/ PS ,w/ PMT cut)	Typical intensity (p.e.)
0.15 m ($\theta \sim 27^\circ \pm 16^\circ$)	NNVT	31.41 (26.27)(12.49)	1.32 (0.93)(0.89)	76
	HPK	13.12 (9.45)(8.97)	0.88 (0.59)(0.59)	30
0.5 m ($\theta \sim 43^\circ \pm 11^\circ$)	NNVT	16.33 (13.01)(7.66)	0.65 (0.42)(0.40)	76
	HPK	11.87 (8.06)(7.71)	0.49 (0.26)(0.26)	31
1.0 m ($\theta \sim 58^\circ \pm 7^\circ$)	NNVT	11.25 (8.37)(5.24)	0.41 (0.26)(0.24)	85
	HPK	8.36 (5.46)(5.12)	0.34 (0.19)(0.19)	33

correlation between the 20-inch PMT and PS1 is shown on the left of Fig. 13, which shows about three regions⁵ and a more complex pattern than that of trigger mode #3 as shown in Fig. 10. The regions 2 and 3 on the 2-D hit-time plot are from the random coincidence between the 20-inch PMT and the PS1, and region 1 is the target range generated by the events going through the 20-inch PMT and the PS1 at the same time, which is confirmed by the relative hit-time difference distribution. The charge spectrum measured with trigger mode #2 of hit-time region 1 is shown on the right of Fig. 13, where all the curves are normalized to the spectrum of PMT dark count. All the plots show consistent results for the muon related events, while the lower part of trigger mode #2 has an obvious increase. It is possibly relate to the natural radioactivity or muon hitting on the PMT glass. Based

⁵The entries out of the aimed hit-time window are mainly from the random coincidence and secondary pulses.

on the results, it is possible that the step 2 is mainly contributed by the muon and natural radioactivity of the surroundings.

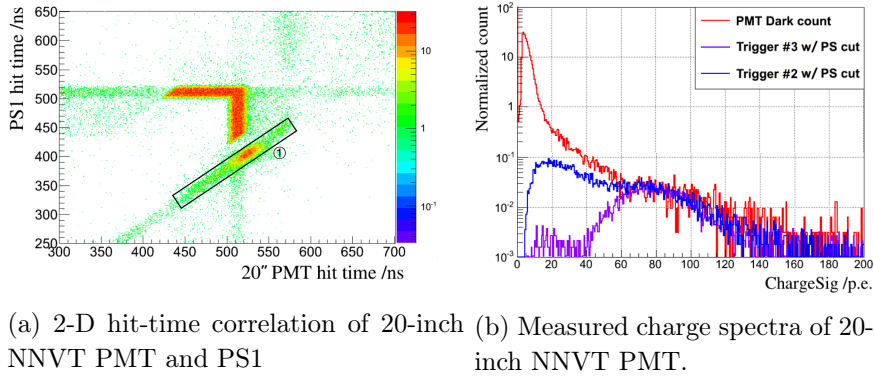


Figure 13: 2-D hit-time correlation between 20-inch NNVT PMT and the PS1 of trigger mode #2 (left) and the measured charge spectra of 20-inch PMTs (right).

3.2.2 PMT photocathode down

Concerning the correlation between the Cerenkov light direction and photocathode acceptance when a muon going through the glass bulb, another special test is done further with the PMT photocathode towards to down (comparing towards to up). The trigger mode #3 is also used for the test only with 20-inch NNVT PMT. The measured charge spectra are shown in Fig. 14 with the raw spectra and after further PSs' offline cut. It also shows obvious muon related events, which is basically consistent with the photocathode directed upwards. But the typical intensity of photocathode towards to down is around 50 p.e. which is only about 66% of photocathode towards to up. The direction of Cerenkov light will affect the PMT acceptance for a muon passing through the PMT glass bulb.

4 Simulation

Geant4[58] is widely used for particle physics detector simulation. A Geant4 simulation of the whole setup with muons passing through the PMT glass bulb was done and compared with the experimental measurements. The results will help on the understanding of the measurements and to prospect the features of this process in the future JUNO detector.

4.1 Simulation setup

The simulation project is setup with the 20-inch PMT (HPK or NNVT) and two plastic scintillators inside a standalone dark box, where all the parameters are configured following the study in [59]. The realized geometry can be found in Fig. 15. The muon generator is based on the muon momentum distribution at sea level [60].

There are few critical configurations to mention:

- (1) Construct the geometry models of PS1, PS2, 20-inch NNVT PMT and HPK PMT, and realize optical processes for Cerenkov radiation in PMT glass. An uniform thickness of PMT glass is used in the simulation.

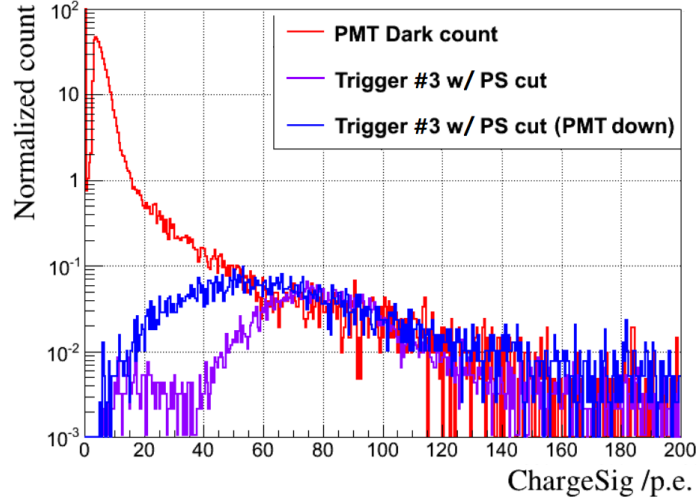


Figure 14: Measured charge spectra of 20-inch NNVT PMT when its photo-cathode towards to down.

- (2) Verify the simulation process related to the PMT glass including Cerenkov radiation (see Fig. 16a) and QE curve of photocathode (see Fig. 16b).
- (3) Muons are generated following the distribution with 4π solid angle randomly on a plane $10 \times 10 \text{ m}^2$ just above PS2.

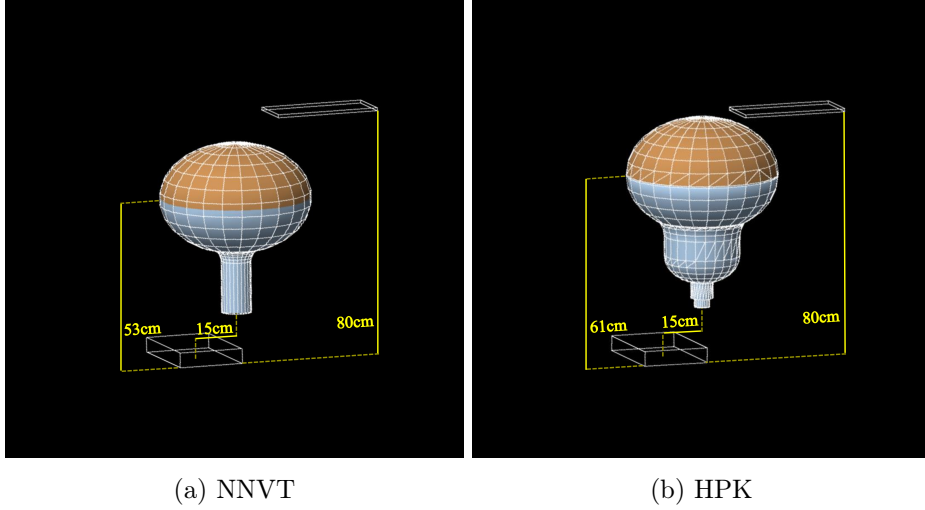
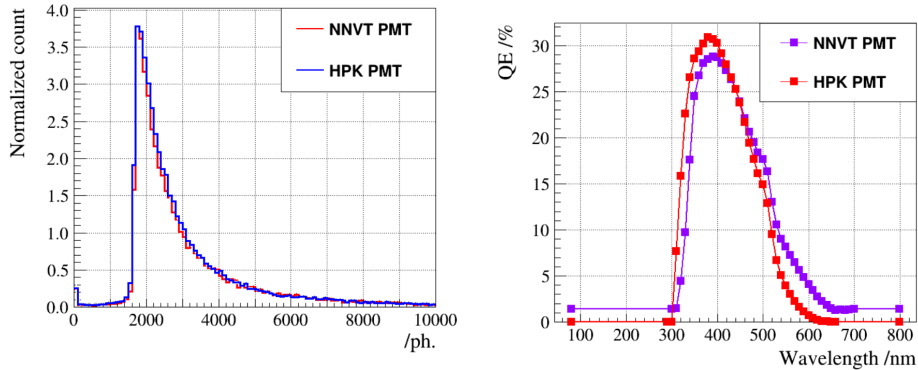


Figure 15: Geometry realized in the simulation for 20-inch NNVT PMT (left), HPK PMT (right) and two plastic scintillators based on Geant4.

Photons will be generated by Cerenkov radiation when a muon is passing through the PMT glass if its speed exceeds the phase velocity of light in the glass. The produced photon number depends on the refractive index (n) of the passing through medium, here the refractive index model of glass. Assume the glass index $n=1.5$ in the wavelength range, the

distribution of generated photon number by muon within the wavelength range of 80 nm-800 nm is shown in Fig. 16a, where the photon production yield is about 274 ph./mm (about 26 ph./mm within 400 nm-700 nm), basically consistent with theoretical calculation.

The used QE curves of the 20-inch PMT[61, 62] are shown in Fig. 16b, where the value of QE at 420 nm is used as a normalization factor (the shape of the QE curve is unchanged.) to check for relative effect of QE. The QE of NNVT PMT shorter than 300 nm is higher than that of HPK PMT, which will result in a higher output strength of NNVT than HPK PMT. In default, the uniform glass thickness is set to 3 mm for both types of PMTs, and the QE at 420 nm is set to 27.3% for NNVT PMT and 30.8% for HPK PMT respectively.



(a) Generated photon by muons corresponds to 6 mm glass (including in and out). (b) QE curves for both NNVT and HPK 20-inch PMTs

Figure 16: Generated photon number by muons (left) and input QE curves (right).

The typical generated number of photons is around 1771-1793 (100%) in wavelength range of [80,800] nm (considering muon in and out of the close shape of the bulb) when a muon going through the PMT glass. The photon number of hitting the photocathode is around 1246-1267 (70%), which is contributed a lot by total reflection from glass to air (outside PMT volume). The final strength on photocathode of NNVT after QE conversion is 45-50 p.e. (2.8%) and that of HPK is 30-36 p.e. (2.0%). As mentioned, the difference between the two types is mainly source from the shape of QE curve, especially the wavelength range of 80-320 nm.

4.1.1 Effect of glass thickness and QE

The glass thickness and QE coefficient of 20-inch PMT have a significant effect on the detected signal strength from the muon related Cerenkov radiation. A survey on glass thickness and QE normalization factor is done individually, as shown in Fig. 17. The output strength of muon related signal is nearly linear to the glass thickness and the QE: ~ 16 p.e./mm for NNVT PMT and ~ 13 p.e./mm for HPK PMT respectively; ~ 8 p.e./2.7% for NNVT PMT and ~ 6 p.e./2.7% for HPK PMT, the difference is mainly from the difference of QE shape of the two PMT types.

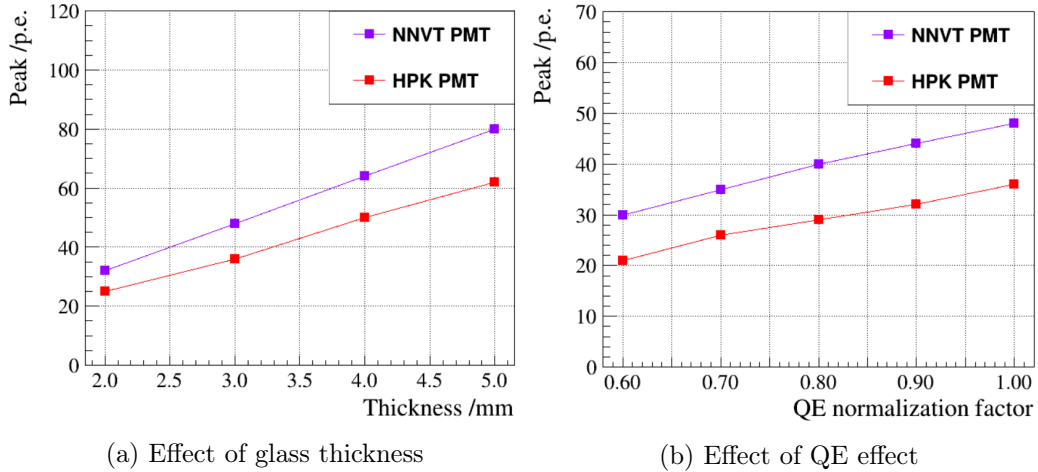


Figure 17: Signal strength from muon versus glass thickness (left) and QE (right) of 20-inch PMT from simulation. The x-axis of right plot is the ratio to default QE.

4.1.2 Simulation for muons

The simulation output is consistent among different trigger modes for both types of PMTs as shown in Fig. 18a for NNVT PMT and Fig. 18b for HPK PMT with $27^\circ \pm 16^\circ$, where all the curves are scaled to a similar statistics around the typical peak. The ratio to only the 20-inch PMT (trigger mode #1) is around 1.9-2.9% with one PS (trigger mode #2) and 0.2% with two PSs (trigger mode #3) respectively. The simulated distribution of detected signal strength by photocathode for different muon angles can be found in Fig. 18c for NNVT PMT and Fig. 18d for HPK PMT with an artificial scale too. The typical values of simulation and measurements are list in Tab. 3, where the original muon rate in simulation is assumed to 200 Hz/m² at ground.

Fig.19 is trying to identify the effect of muon direction or muon hitting location on PMT glass shown in Fig. 18a and Fig. 18b further. The muons hitting the PMT glass are separated into two groups: the muons hitting the PMT photocathode (tagged by "Hit photocathode") and the muons not hitting the PMT photocathode (tagged by "Not hit photocathode"). It shows that even the muon is not hitting the PMT glass with photocathode directly (only passing though the other end of the glass bulb), the PMT still can "see" the photons from the muon. The total refraction effect of PMT glass is helping in this case. The shape difference of the charge spectra between NNVT and HPK PMTs for "Not hit photocathode" is mainly source from the different shape of PMT glass bulb of the two types of PMTs as shown in Fig.15.

The rate and the signal strength both of the measurement and simulation show in Tab. 3, where the measured rate of 20-inch PMT is scaled after a charge cut larger than 40 p.e. for NNVT PMT and 10 p.e. for HPK PMT as discussed. The simulation shows a more narrow distribution than measurements where the height of y-axis is artificial normalized, and the measurements have a long tail than the simulation. As discussed in Sec. 2.2, here the charge in p.e. is calculated with the peak gain, which has a large bias for the

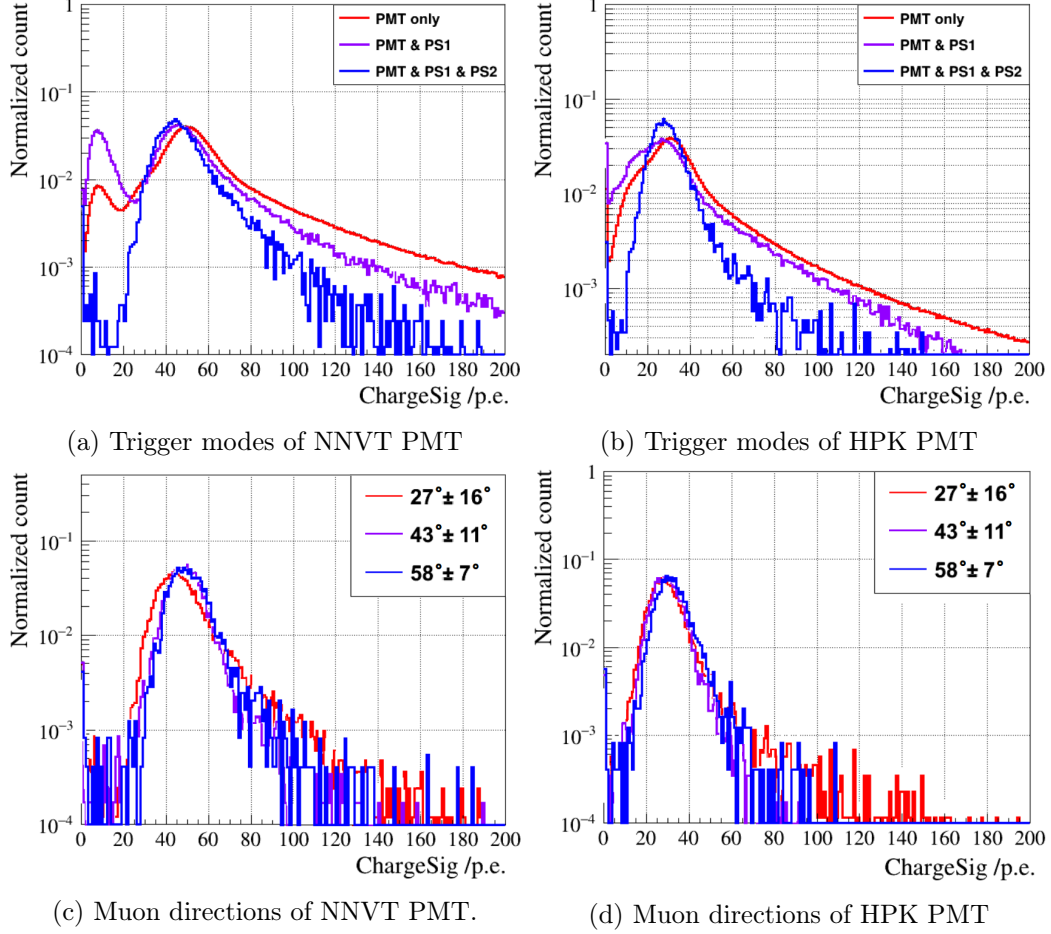


Figure 18: Typical output from simulation of 20-inch PMTs. Top left: simulation of NNVT PMT for $27^\circ \pm 16^\circ$; top right: simulation of HPK PMT for $27^\circ \pm 16^\circ$; bottom left: simulated signal strength of different angles of NNVT PMT; bottom right: simulated signal strength of different angles of HPK PMT.

NNVT PMT[56]. A corrected signal strength⁶ also updated in Tab. 3 tagged by "Cor.", which is more consistent with simulation. Fig. 20a and Fig. 20b show the charge spectra comparison between simulation and measurements which is normalized to the higher part of each curves, while the NNVT result is scaled with the gain factor already.

4.2 Comparison of PMT photocathode up and down

The simulation of the NNVT PMT photocathode towards to down and up is shown in Fig. 20c for NNVT PMT. The reason is similar to that shown in Fig. 19 that the effect of total reflection from PMT glass to air or vacuum is confirmed. While the collected photon number of PMT photocathode towards to down is less than that of PMT photocathode towards to up. It is around 76% of the output of photocathode towards to down to photocathode towards to up, which is basically consistent with the measurement.

⁶Here the gain factor 1.6 is used according to [56].

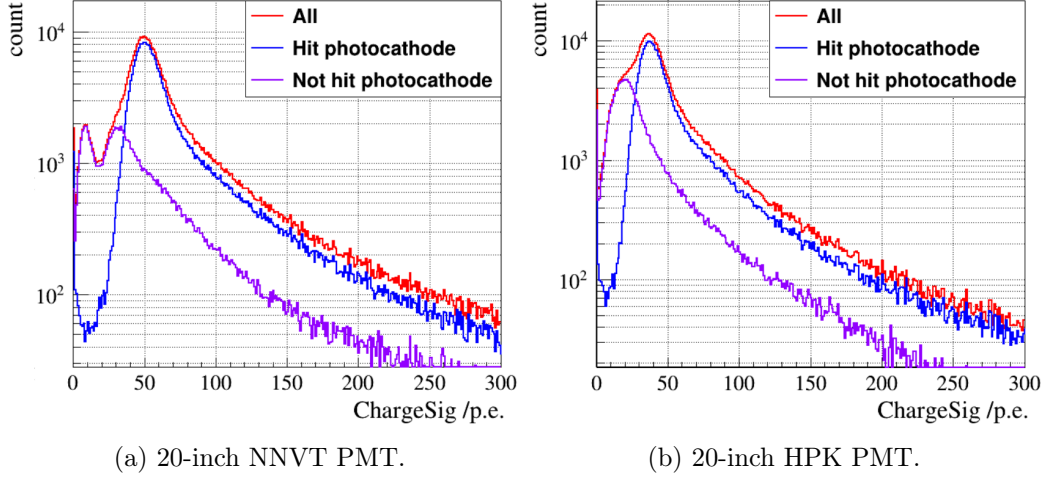


Figure 19: Effect of muon hitting location: passing through or not the photocathode of 20-inch PMTs.

Table 3: Comparison of simulation and measurement at zenith angle $\theta = 27^\circ \pm 16^\circ$ of trigger mode #3. The rate of the simulation is counted in three columns: the total muon hit rate (tagged by "all"), the muon hit rate passing the photocathode (tagged by "photo-") and the muon hit rate not passing the photocathode (tagged by "not photo-"). The rate of PMT only of the measurement is counted only in the range of >40 p.e. for NNVT, >10 p.e. for HPK, with the PS offline cut.

PMT	Config. (trig. mod.)	Sim. (p.e.)	Test (Cor.) (p.e.)	Sim. rate (all)(Hz)	Sim. rate (photo-)	Sim. rate (not photo-)	Test rate (Hz)
	20" only (#1)	50	/ (/)	77.98	56.86	21.12	69.33
NNVT	20" & PS1 (#2)	47	79 (49)	2.24	1.41	0.83	12.49
	20" & PS1 & PS2 (#3)	45	76 (47.5)	0.18	0.17	0.01	0.89
	20" only (#1)	36	/	87.04	57.57	29.47	75.19
HPK	20" & PS1 (#2)	32	34	1.69	1.03	0.66	8.97
	20" & PS1 & PS2 (#3)	30	33	0.17	0.14	0.03	0.59

5 Summary

In this paper, we investigated the large pulses of 20-inch PMT dark count, which are mainly from the muons crossing through the PMT glass which generate some large pulses

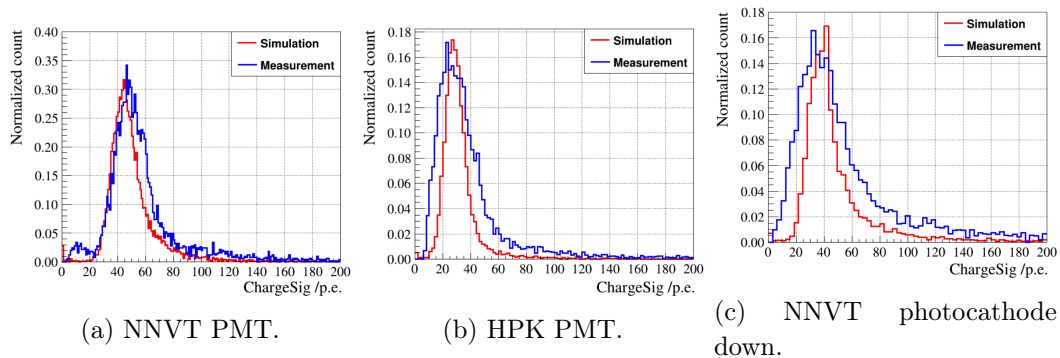


Figure 20: Comparison between the measurements and the simulation of 20-inch PMTs.

with Cerenkov radiation for both types of dynode and MCP PMTs, and compared their charge responses between the measured and simulated charge spectra. We setup a waveform data taking system to get the muon related PMT large pulse in dark with a setup of muon coincidence system, which is extracted from the peak location of the single photoelectron at different zenith angles, for both PMT types. It is also concluded that the large pulses detected by PMT are able to be interpreted in conjunction with muon hitting PMT at recent world-wide neutrino experiments. It is also confirmed that the signal strength related to muons of photocathode down is smaller than photocathode up, but the difference of muon zenith angles has little effect. It is also confirmed that the charge output of both types of PMTs is linear to the PMT glass thickness and QE coefficient.

Acknowledgements

This work was supported by the National Natural Science Foundation of China No. 11875282, the Strategic Priority Research Program of the Chinese Academy of Sciences (Grant No. XDA100102).

References

- [1] Zelimir Djurcic et al. JUNO Conceptual Design Report. *arXiv e-prints*, 8 2015.
- [2] F. An et al. Neutrino Physics with JUNO. *J. Phys. G*, 43(3):030401, 2016. doi: 10.1088/0954-3899/43/3/030401.
- [3] JUNO collaboration. JUNO physics and detector. *Progress in Particle and Nuclear Physics*, 123:103927, 2022. ISSN 0146-6410. doi: <https://doi.org/10.1016/j.ppnp.2021.103927>. URL <https://www.sciencedirect.com/science/article/pii/S0146641021000880>.
- [4] L. Wen et al. A quantitative approach to select PMTs for large detectors. *Nucl. Instrum. Meth. A*, 947:162766, 2019. doi: 10.1016/j.nima.2019.162766.
- [5] Z. Qin. Status of the 20-in. PMT Instrumentation for the JUNO Experiment. In *Proceedings of International Conference on Technology and Instrumentation in Particle Physics 2017*, pages 285–293. Springer Singapore, 2018. ISBN 978-981-13-1316-5.

- [6] Hamamatsu Photonics K.K. R12860 datasheet, 2019. <https://www.hamamatsu.com/jp/en/product/type/R12860/index.html>.
- [7] Northern Night Vision Technology Ltd. Specification for GDB-6201 microchannel plate type photomultiplier PMT (in Chinese), 2020. <https://max.book118.com/html/2020/0214/7002125152002115.shtm>.
- [8] Y. Fukuda et al. Measurement of the flux and zenith angle distribution of upward through going muons by Super-Kamiokande. *Phys. Rev. Lett.*, 82:2644–2648, 1999. doi: 10.1103/PhysRevLett.82.2644.
- [9] Abe K. et al. Solar neutrino results in Super-Kamiokande-III. *Phys. Rev. D*, 83:052010, Mar 2011. doi: 10.1103/PhysRevD.83.052010. URL <https://link.aps.org/doi/10.1103/PhysRevD.83.052010>.
- [10] Eguchi, K. et al. First Results from KamLAND: Evidence for Reactor Antineutrino Disappearance. *Phys. Rev. Lett.*, 90:021802, Jan 2003. doi: "10.1103/PhysRevLett.90.021802".
- [11] Ahmad QR, Allen RC, Andersen TC, et al. Measurement of day and night neutrino energy spectra at SNO and constraints on neutrino mixing parameters. *Phys Rev Lett.*, 89(1): 011302, 2002. doi: {10.1103/PhysRevLett.89.011302}.
- [12] Thierry Lasserre. The reactor antineutrino anomaly. *Journal of Physics Conference Series*, 375:2042–, 07 2012. doi: 10.1088/1742-6596/375/1/042042.
- [13] Aartsen, M. G. et al. Search for Dark Matter Annihilations in the Sun with the 79-String IceCube Detector. *Phys. Rev. Lett.*, 110:131302, Mar 2013. doi: 10.1103/PhysRevLett.110.131302.
- [14] "Abe Y and others". Indication of reactor $\nu(e)$ disappearance in the Double Chooz experiment. "*Phys Rev Lett.*", "108"("13"):"131801", "2012". doi: "10.1103/PhysRevLett.108.131801".
- [15] An FP et al. Observation of electron-antineutrino disappearance at Daya Bay. *Phys Rev Lett.*, 108(17):171803, 2012. doi: 10.1103/PhysRevLett.108.171803.
- [16] Soo-Bong Kim. Observation of Reactor Electron Antineutrino Disappearance at RENO. *Nuclear Physics B - Proceedings Supplements*, 235-236:24–29, 2013. ISSN 0920-5632. doi: 10.1016/j.nuclphysbps.2013.03.006.
- [17] D. Barnhill et al. Testing of photomultiplier tubes for use in the surface detector of the Pierre Auger Observatory. *Nucl. Instrum. Meth. A*, 591:453–466, 2008. doi: 10.1016/j.nima.2008.01.088.
- [18] Maomao Ge, Li Zhang, Yingtao Chen, Zhen Cao, Shoushan Zhang, Chong Wang, and Baiyang Bi. Photomultiplier tube selection for the wide field of view cherenkov/fluorescence telescope array of the large high altitude air shower observatory. *Nuclear Instruments and Methods in Physics Research Section A*, 819:175–181, 2016. doi: 10.1016/j.nima.2016.02.093.
- [19] G. Ranucci et al. Characterization and magnetic shielding of the large cathode area PMTs used for the light detection system of the prototype of the solar neutrino experiment Borexino. *Nucl. Instrum. Meth. A*, 337:211–220, 1993. doi: 10.1016/0168-9002(93)91156-H.
- [20] D. Liu. PMT evaluation for the Daya Bay neutrino experiment. In *2008 IEEE Nuclear Science Symposium and Medical Imaging Conference and 16th International Workshop on*

Room-Temperature Semiconductor X-Ray and Gamma-Ray Detectors, pages 3133–3139, 2008. doi: 10.1109/NSSMIC.2008.4775017.

- [21] A. Baldini et al. The photomultiplier test facility for the reactor neutrino oscillation experiment CHOOZ and the measurements of 250 8-in. EMI 9356KA B53 photomultipliers. *Nucl. Instrum. Meth. A*, 372(1):207–221, 1996. doi: [https://doi.org/10.1016/0168-9002\(95\)01236-2](https://doi.org/10.1016/0168-9002(95)01236-2).
- [22] C. Bronner et al. Development and performance of the 20" PMT for Hyper-Kamiokande. *J. Phys. Conf. Ser.*, 1468(1):012237, 2020. doi: 10.1088/1742-6596/1468/1/012237.
- [23] C. Cao et al. Mass production and characterization of 3-inch PMTs for the JUNO experiment. *Nucl. Instrum. Meth. A*, 1005:165347, 2021. doi: 10.1016/j.nima.2021.165347.
- [24] C. M. Mollo. Development and performances of a high statistics PMT test facility. *EPJ Web Conf.*, 116:06010, 2016. doi: 10.1051/epjconf/201611606010.
- [25] A. Yang et al. Study and removal of the flash from the HV divider of the 20-inch PMT for JUNO. *JINST*, 15(04):T04006, 2020. doi: 10.1088/1748-0221/15/04/T04006.
- [26] S. Qian et al. The improvement of 20" MCP-PMT for neutrino detection. *PoS, ICHEP2018*: 662, 2019. doi: 10.22323/1.340.0662.
- [27] Y. Wang et al. A new design of large area MCP-PMT for the next generation neutrino experiment. *Nucl. Instrum. Meth. A*, 695:113–117, 2012. doi: 10.1016/j.nima.2011.12.085.
- [28] S. Yin et al. A novel PMT test system based on waveform sampling. *JINST*, 13(01):T01005, 2018. doi: 10.1088/1748-0221/13/01/T01005.
- [29] H. Q. Zhang et al. Comparison on PMT Waveform Reconstructions with JUNO Prototype. *JINST*, 14(08):T08002, 2019. doi: 10.1088/1748-0221/14/08/T08002.
- [30] Y. Abe et al. Characterization of the spontaneous light emission of the PMTs used in the double chooz experiment. *Journal of Instrumentation*, 11(08):P08001–P08001, aug 2016. doi: 10.1088/1748-0221/11/08/p08001.
- [31] D.A. Dwyer. Improved measurement of electron-antineutrino disappearance at daya bay. *Nuclear Physics B*, 235-236:30–32, 2013. doi: 10.1016/j.nuclphysbps.2013.03.007.
- [32] D. van Eijk, J. Schneider, and M. Unland. Characterisation of Two PMT Models for the IceCube Upgrade mDOM. *PoS, ICRC2019*:1022, 2020. doi: 10.22323/1.358.1022.
- [33] J.S. Jang. A precise measurement of reactor antineutrino at reno. *Nuclear Data Sheets*, 120: 145–148, 2014. ISSN 0090-3752. doi: 10.1016/j.nds.2014.07.030.
- [34] A. Yang, Z. Qin, Z. Wang, H. Chen, W. Wei, F. Luo, M. Xu, Y. Heng, and Q. Ouyang. Study and removal of the flash from the HV divider of the 20-inch PMT for JUNO. *Journal of Instrumentation*, 15(04):T04006–T04006, apr 2020. doi: 10.1088/1748-0221/15/04/t04006.
- [35] Sen Qian, Feng Gao, Lishuang Ma, Yao Zhu, Shanhong Chen, and Pengyu Chen. The study on the 20 inch PMT flasher signal. *Journal of Instrumentation*, 15(06):T06008–T06008, 2020. doi: 10.1088/1748-0221/15/06/t06008.
- [36] L. Villasenor" "W. Raposo, M. Vaz. "measurements of signals from muons crossing the hamamatsu r5912 pmt enclosure vertically and horizontally". *online*, "2007". "AngraNote 004-2007".
- [37] E. Bayat, V. Doust-Mohammadi, P. Ghorbani, N. Ghal-Eh, and R. Mohammadi. Scintillation of xp2020 pmt glass window. *Radiation Physics and Chemistry*, 102:1–4, 2014.

ISSN 0969-806X. doi: <https://doi.org/10.1016/j.radphyschem.2014.04.009>. URL <https://www.sciencedirect.com/science/article/pii/S0969806X14001285>.

- [38] Hyper-Kamiokande Proto-Collaboration, Abe K, et al. Hyper-Kamiokande Design Report. *arXiv e-prints*, art. arXiv:1805.04163, May 2018.
- [39] K. et al. Abe. Physics potential of a long-baseline neutrino oscillation experiment using a J-PARC neutrino beam and Hyper-Kamiokande. *Progress of Theoretical and Experimental Physics*, 2015(5), 05 2015. doi: 10.1093/ptep/ptv061. URL <https://doi.org/10.1093/ptep/ptv061>. 053C02.
- [40] Shanghai TT112. thickness meter TT112, 2021. <http://www.jsbyb.com/wujiu-Products-4070951/>.
- [41] Ken Chow et al. Waterproofed photomultiplier tube assemblies for the daya bay reactor neutrino experiment. *Nuclear Instruments and Methods in Physics Research Section A*, 794: 25–32, 2015. doi: 10.1016/j.nima.2015.05.002.
- [42] Photonis. Standard very fast, 12-stage, 51 mm (2") round tube, 1998. URL <https://irfu.cea.fr/dphn/Tp/xp2020.pdf>.
- [43] CAEN SpA. DT5751, 2/4 channel 10 bit 2/1 gs/s digitizer, 2021. <https://www.caen.it/products/dt5751/>.
- [44] iseg Spezialelektronik GmbH company. SHR, switchable high end high precision ac/dc desktop hv source-measure-unit, 2021. <https://iseg-hv.com/en/products/detail/SHR>.
- [45] CAEN SpA. N625, quad linear fan-in fan-out, 2021. <https://www.caen.it/products/n625/>.
- [46] CAEN SpA. N979, 16 channel fast amplifier, 2021. <https://www.caen.it/products/n979/>.
- [47] CAEN SpA. N845, 16 channel low threshold discriminator, 2021. <https://www.caen.it/products/n845/>.
- [48] CAEN SpA. N1145, quad scaler and preset counter/timer, 2021. <https://www.caen.it/products/n1145/>.
- [49] CAEN SpA. N455, quad coincidence logic unit, 2021. <https://www.caen.it/products/n455/>.
- [50] F. Luo et al. Signal Optimization with HV divider of MCP-PMT for JUNO. *Springer Proc. Phys.*, 213:309–314, 2018. doi: 10.1007/978-981-13-1316-5_58.
- [51] F. Luo et al. PMT overshoot study for the JUNO prototype detector. *Chin. Phys. C*, 40(9): 096002, 2016. doi: 10.1088/1674-1137/40/9/096002.
- [52] Sergey V. Polyakov. Chapter 3 - photomultiplier tubes. In Alan Migdall et al., editor, *Single-Photon Generation and Detection*, volume 45 of *Experimental Methods in the Physical Sciences*, pages 69–82. Academic Press, 2013. doi: 10.1016/B978-0-12-387695-9.00003-2.
- [53] E. H. Bellamy et al. Absolute calibration and monitoring of a spectrometric channel using a photomultiplier. *Nucl. Instrum. Meth. A*, 339:468–476, 1994. doi: 10.1016/0168-9002(94)90183-X.
- [54] F. Luo et al. A study of the new hemispherical 9-inch PMT. *Journal of Instrumentation*, 14 (02):T02004–T02004, feb 2019. doi: 10.1088/1748-0221/14/02/t02004. URL <https://doi.org/10.1088/1748-0221/14/02/t02004>.
- [55] R. Saldanha et al. Model Independent Approach to the Single Photoelectron Calibration of Photomultiplier Tubes. *Nucl. Instrum. Meth. A*, 863:35–46, 2017. doi: 10.1016/j.nima.2017.02.086.

- [56] H. Q. Zhang et al. Gain and charge response of 20" MCP and dynode PMTs. *JINST*, 16(08): T08009, 2021. doi: 10.1088/1748-0221/16/08/T08009.
- [57] Hamamatsu Photonics K.K. *Photomultiplier Tubes - Basics and Applications*. Hamamatsu Photonics K.K., 3rd edition, 2007.
https://www.hamamatsu.com/resources/pdf/etd/PMT_handbook_v3aE.pdf.
- [58] Geant4 Working Groups & Coordinators. Geant4, 2021. <https://geant4.web.cern.ch/>.
- [59] Tao Lin et al. The application of SNiPER to the JUNO simulation. *Journal of Physics: Conference Series*, 898:042029, oct 2017. doi: 10.1088/1742-6596/898/4/042029. URL <https://doi.org/10.1088/1742-6596/898/4/042029>.
- [60] Mengyun Guan, Ming chung Chu, Jun Cao, K. B. Luk, and Chang gen Yang. A parametrization of the cosmic-ray muon flux at sea-level. *arXiv: High Energy Physics - Experiment*, 2015.
- [61] H. Zhang et al. Study on relative collection efficiency of PMTs with spotlight. *Radiat. Detect. Technol. Methods*, 3:20, 2019. doi: 10.1007/s41605-019-0099-x.
- [62] X.-C. Lei et al. Evaluation of new large area PMT with high quantum efficiency. *Chin. Phys. C*, 40(2):026002, 2016. doi: 10.1088/1674-1137/40/2/026002.